

Quantum communications in a moderate-to-strong turbulent space

Masoud Ghalaii (✉ masoud.ghalaii@york.ac.uk)

University of York <https://orcid.org/0000-0002-4242-8748>

Stefano Pirandola

University of York <https://orcid.org/0000-0001-6165-5615>

Article

Keywords: refraction, atmospheric extinction, pointing errors and, most importantly, turbulence

Posted Date: August 9th, 2021

DOI: <https://doi.org/10.21203/rs.3.rs-754127/v1>

License:  This work is licensed under a Creative Commons Attribution 4.0 International License.

[Read Full License](#)

Version of Record: A version of this preprint was published at Communications Physics on February 10th, 2022. See the published version at <https://doi.org/10.1038/s42005-022-00814-5>.

Quantum communications in a moderate-to-strong turbulent space

Masoud Ghalaii and Stefano Pirandola

Department of Computer Science, University of York, York YO10 5GH, United Kingdom

Since the invention of the laser in the 60s, one of the most fundamental communication channels has been the free-space optical channel. For this type of channel, a number of effects generally need to be considered, including diffraction, refraction, atmospheric extinction, pointing errors and, most importantly, turbulence. Because of all these adverse features, the free-space channel is more difficult to study than a stable fiber-based link. For the same reasons, only recently it has been possible to establish the ultimate performances achievable in quantum communications via free-space channels, together with practical rates for continuous variable (CV) quantum key distribution (QKD). Differently from previous literature, mainly focused on the regime of weak turbulence, this work considers the free-space optical channel in the more challenging regime of moderate-to-strong turbulence, where effects of beam widening and breaking are more important than beam wandering. This regime may occur in long-distance free-space links on the ground, in uplink to high-altitude platform systems (HAPS) and, more interestingly, in downlink from near-horizon satellites. In such a regime we rigorously investigate ultimate limits for quantum communications and show that composable keys can be extracted using CV-QKD. In particular, we apply our results to downlink from satellites at large zenith angles, for which not only turbulence is strong but also refraction causes non-trivial effects in terms of trajectory elongation.

Yearslong chain of excellent work have stitched quantum communications and quantum cryptography into the science of quantum information technologies. In particular, quantum key distribution (QKD) [1] has been developing rapidly, with the end goal of making distant individuals able to share a key, which must be inscrutable for an eavesdropper to learn about, and which, therefore, can be used for secure classical communications. Since 1980s that saw the debut of QKD [2], optical fibers have been the main platform to perform and/or experiment most QKD protocols. However, the reach of fiber-based quantum communications is limited to only a few hundreds of kilometers [3–6] (because of the exponential decay of the transmissivity). Whereas, man seems to stand on the verge of building a quantum internet [7, 8] to make global quantum communications viable for all. Therefore, as a possible solution, one may think of a harmonized use of quantum repeater stations (placed on ground and connected via optical fibers) and free-space optical (FSO) communication links. The latter include ground-to-ground free-space channels [9] and HAPS, downlink/uplink communications with satellites [10, 11], and inter-satellite links [12] (see Ref. [13] for a review).

It is desirable to find the limits of quantum communications and QKD in different types of free-space medium, such as the Earth’s atmosphere and space. In fact, alike the PLOB bound [14] and quantum repeater capacities [15], one may work out bounds germane to free-space and satellite links, where the most detrimental phenomena is perhaps, not surprisingly, turbulence—fluctuations in the atmosphere refractive index due to the aerodynamics and temperature gradient of the Earth’s surface [16, 17]. Due to atmospheric turbulence the spatial coherence of an optical beam is gradually destroyed as it propagates. This loss of spatial coherence restricts the reach to which beams can be focused or collimated [18–20]. This in turn results in significant power level reductions in FSO communication and radar links. Equally fatal, the destruction of coherence can effect optical receivers, which are very sensitive to the loss of spatial coherence [21, 22].

Accounting for realistic effects on optical beams, such as diffraction, extinction, background noise, and channel fading,

the latter due to pointing errors and atmospheric turbulence, Pirandola investigated the ultimate quantum communication limits and the practical security of FSO links, considering ground-based communications [23] and uplink/downlink with satellites [24]. Even though the theory developed in Ref. [23] is very general, the main focus was the regime of weak turbulence, suitable for short-range high-rate FSO links on the ground. Similarly, the main focus of Ref. [24] was quantum communications with satellites within 1 radian from the zenith position, so to enforce the regime of weak fluctuations.

In this manuscript, we extend the investigation to the regime of moderate-to-strong turbulence [22, 25–27], where optical waves can harshly be deformed and eventually broken up into multiple patches [22, 28], such that one would observe a random multiplicity of spots distributed on the receiving aperture [29, 30]. In this more challenging regime, we provide information-theoretic bounds for the maximum rates that are achievable for key generation and entanglement distribution. We then study the composable finite-size key rates that can be achieved by protocols of CV-QKD, showing the feasibility of this approach in moderate-to-strong FSO links.

The considered stronger regime of turbulence occurs in long-distance free-space connections on the ground but also, and more interestingly, in communications with satellites at large zenith angles (beyond 1 radian). When a satellite is close to the horizon, the optical path within Earth’s atmosphere becomes long and turbulence becomes a major problem. At these angles, another problem is refraction, which creates an elongation of the atmospheric section of the path (and therefore further loss and turbulence occur). Accounting for all these adverse aspects, we bound the optimal performances and provide achievable key rates.

RESULTS

We first present some preliminary aspects and physics of FSO communications in turbulent media. We shall use these in the rest of the paper in order to understand and establish both ultimate limits and practical security of quantum communications in a moderate-to-strong turbulent space.

Figure of merit for the strength of turbulence. AS-146
 96 some an optical-beam signal of wavelength λ that propagates 147
 97 through a turbulent path of length z . As widely accepted, 148
 98 [16, 22, 25], we introduce the Rytov number to be the fig- 149
 99 ure of merit for the strength of turbulence. Physically, the 150
 100 Rytov number, or Rytov variance, is a measure of the strength 151
 102 of light scintillations—fluctuations in received irradiance, or 152
 103 in the phase and amplitude of the light, resulting from propa- 153
 104 gation through a turbulent space [16, 31]. The dimensionless 154
 105 Rytov number is defined for a plane wave as follows [32]

$$\sigma_{\text{Ry}}^2 = 1.23 C_n^2 k^{\frac{7}{6}} z^{\frac{11}{6}}, \quad (1)_{153, 154}$$

106 where $k = 2\pi/\lambda$ is the wavenumber and C_n^2 is known as the 155
 107 index-of-refraction structure constant, measuring the magni- 156
 108 tude of the fluctuations in the index of refraction (the Rytov 157
 109 number for a spherical wave is $0.4\sigma_{\text{Ry}}^2$). It is interesting to note 158
 110 that the scintillation of an optical signal does not increase un- 159
 111 limitedly as predicted by Rytov approximation [32], but satu- 160
 112 rates for strong turbulence and long propagation links [22]. It 161
 113 can nevertheless still specify turbulence regimes. 162

114 Values of $\sigma_{\text{Ry}}^2 < 1$ refer to weak turbulent media, while 163
 115 $\sigma_{\text{Ry}}^2 > 1$ indicate strong turbulence [25]. The regime of inter- 164
 116 mediate turbulent media hence is lying around $\sigma_{\text{Ry}}^2 \sim 1$. Rytov 165
 117 number is very much similar to the dimensionless Reynolds 166
 118 number [33], Re , in fluid mechanics, where for a fluid flow- 167
 119 ing through a packed bed of particles $Re < 10$ corresponds 168
 120 to a laminar flow, whereas $Re > 2000$ indicates a turbulent 169
 121 stream [34]. According to the Rytov number, the specification 170
 122 of turbulence regimes involves not just the index-of-refraction 171
 123 structure constant C_n^2 , but a combination of this parameter, the 172
 124 beam's wavelength and the propagation path length. 173

125 The positive power dependence of the Rytov number on 174
 126 path length z implies that the medium is indeed expected to be 175
 127 highly turbulent at longer distances [22]. It is hence helpful to 176
 128 introduce another quantity which is relevant to the propaga- 177
 129 tion distance, which is [25, 27, 35] 178

$$z_i = (C_n^2 k^2 \ell_0^{5/3})^{-1}. \quad (2)_{177, 178}$$

130 Parameter z_i represents the propagation length at which the 179
 131 transverse coherence radius of the optical wave is comparable 180
 132 to the turbulence inner scale ℓ_0 . The parameter ℓ_0 , which is on 181
 133 the order of 1 mm, is a measure of the smallest distances over 182
 134 which fluctuations in the index of refraction are correlated. 183
 135 We will shortly discuss that z_i defines the minimum valid dis- 184
 136 tance for some relevant quantities in studying stronger turbu- 185
 137 lence media; that is, some equations are sound only for $z > z_i$. 186
 138 Fortunately, apropos equations can be found in the literature 187
 139 for $z < z_i$, where we may expect a moderate or strong turbu- 188
 140 lence space. It is worth mentioning that, in the regime of weak 189
 141 turbulence, a similar quantity, known as the spatial coherence 190
 142 radius $\rho_0 = (iC_n^2 k^2 z)^{-\frac{3}{5}}$, is introduced, where $i = 0.55$ (1.46)
 143 corresponds to plane (spherical) waves [16].

144 **Pure diffraction and optical loss in free space.** A natural 191
 145 light's phenomenon is diffraction, which perennially spreads

the wave's size while it propagates through free space. It also
 constantly increases the radius of curvature of the propagating
 beam [19, 20]. In our study, we start with a Gaussian beam,
 with initial field spot size w_0 , carrier wavelength λ , and ra-
 dius of curvature R_0 . At distance z of propagation, where a
 receiver is supposedly placed, free-space diffraction increases
 the beam's spot size to

$$w_z^2 = w_0^2 \left[\left(1 - \frac{z}{R_0}\right)^2 + \left(\frac{z}{z_R}\right)^2 \right], \quad (3)$$

with $z_R = \pi w_0^2/\lambda$ being the beam's Rayleigh length. A re-
 ceiver with infinite radius would collect all the light. However,
 practically speaking, only a fraction of the light can be col-
 lected by a receiver with a realistic finite aperture with radius
 a_R . This defines the pure diffraction-induced transmissivity

$$\eta_{\text{dif}} = 1 - e^{-\frac{2a_R^2}{w_z^2}}, \quad (4)$$

yet, in reality, this would not be the total loss in a turbulent
 atmosphere as we shall see below.

Turbulence-induced beam spread. Equation (4) can lead
 to incorrect estimations because of Eq. (3), which may under-
 estimate the effective spot size of the beam. This is because
 a different physics setting may apply in many real-world sce-
 narios due to atmospheric turbulence. Therefore, we need to
 provide a proper estimation of the z -dependent spot size in
 order to modify η_{dif} in Eq. (4). In a moderate-to-strong tur-
 bulent regime, a beam can breakup into multiple patches and
 this primarily happens at longer propagation distances, where
 it is expected to have a large Rytov number. In this case, the
 patches of the beam will be in an area with mean square radius
 w_{lt}^2 , also known as the *long-term beam waist* [22]. Note that
 the relevant beam spread in the regime of weak turbulence is
 the short-term beam waist, w_{st}^2 [27]. In general, one has the
 decomposition $w_{\text{lt}}^2 = w_{\text{st}}^2 + \sigma_{\text{tb}}^2$ [23, 25, 27], where σ_{tb}^2 is the
 variance associated with the wandering of the beam centroid.
 However, for stronger turbulence, wandering becomes negligi-
 ble with respect to beam widening, i.e., we have the collapse
 $\sigma_{\text{tb}}^2 \ll w_{\text{st}}^2 \simeq w_{\text{lt}}^2$. See Fig. 1 for a study of these quantities.

Let us now assume a Gaussian beam with initial spot radius
 w_0 and curvature R_0 . After travelling through a path of length
 z , such a beam is characterized by a pair of parameters [16, 36]

$$\Omega_0 = 1 - \frac{z}{R_0}, \quad \Lambda_0 = \frac{2z}{k w_0^2}. \quad (5)$$

For example, the pair $\Omega_0 = 0$ and $\Lambda_0 = 0$ corresponds to
 a spherical wave, whereas $\Omega_0 = 1$ and $\Lambda_0 = 0$ represents a
 plane wave. Alternatively, in the plane of the receiver, such a
 Gaussian beam can be described by the similar pair of param-
 eters

$$\Omega = \frac{\Omega_0}{\Omega_0^2 + \Lambda_0^2} = 1 + \frac{z}{R}, \quad \Lambda = \frac{\Lambda_0}{\Omega_0^2 + \Lambda_0^2} = \frac{2z}{k w_z^2}, \quad (6)$$

187 where R is the phase front radius of curvature at the receiver.
 188 It is then shown that, at distances $z > z_i$, where a strong tur-
 189 bulent space is experienced [22], the long-term beam waist at
 190 the receiver is given by [16, Chap. 8]

$$w_{lt} = w_z \sqrt{1 + \frac{4}{3} q \Lambda}, \quad (7)$$

191 with the q parameter equal to

$$q = 0.74 \sigma_{Ry}^2 Q_m^{1/6}, \quad Q_m = 35.05 z / (k \ell_0^2). \quad (8)$$

192 In Eq. (7), we see how the diffraction-limited beam waist w_z
 193 is revised into the long-term beam waist w_{lt} via an additional
 194 spread factor associated with scattering by turbulent eddies.

195 Note that even through a short propagation distance the
 196 beam may experience a moderate or strong turbulence space.
 197 In this case ($z < z_i$) the effective beam waist is

$$w_{lt} = w_z \sqrt{1 + 1.63 (\sigma_{Ry}^2)^{6/5} \Lambda}. \quad (9)$$

198 The above equation is also considered to be adequately precise
 199 for weak turbulence so that it can generally be used to estimate
 200 the long-term beam waist under almost all turbulence condi-
 201 tions. Thus, we may use Eq. (9) at all distances $0 \approx z < z_i$, no
 202 matter of the strength of turbulence. 228

203 In this study, Eqs. (7) and (9) provide the main quantities
 204 that we shall use to bound the rate of quantum communica-
 205 tions in a moderate-to-strong turbulent space. 231

206 **More details on beam wandering.** While transmitting an
 207 optical signal through free space, it is observed that position
 208 of the instantaneous centroid of the signal (point of maximum
 209 irradiance or “hot spot”) is randomly displaced. This instan-
 210 taneous quivering in the plane of the receiver, which supposedly
 211 happens according to a Gaussian distribution with variance
 212 σ^2 , is commonly called beam or centroid wandering. Overall,
 213 this wandering is caused by pointing error σ_{pe}^2 , due to Gaus-
 214 sian jitter and off-target tracking, and atmospheric turbulence
 215 σ_{tb}^2 . These two effects are independent and sum up such that
 216 the total variance of the wandering is given by $\sigma^2 = \sigma_{pe}^2 + \sigma_{tb}^2$.
 217 The amount of wandering for a typical $1 \mu\text{rad}$ off-tracking
 218 error at the transmitter is given by $\sigma_{pe}^2 \approx 10^{-12} z^2$. But, the
 219 contribution of atmospheric turbulence is more elaborate. 244

220 Different mathematical expressions have been developed to
 221 estimate wandering in strong turbulent media [16, 25, 26, 28].
 222 Here, we use the following estimation [16, Chap. 8] 247

$$\sigma_{tb}^2 = 7.25 C_n^2 w_0^{-1/3} z^3 \int_0^1 d\xi \left[\frac{1}{f^{1/6}(\xi)} - \frac{\kappa_0^{1/3} w_0^{1/3}}{[1 + \kappa_0^2 w_0^2 f(\xi)]^{1/6}} \right], \quad (10)$$

223 where $\kappa_0 = 2\pi/L_0$, with $L_0 \approx 1 - 100$ m being the outer scale
 224 of turbulence and 256

$$f(\xi) = [\Omega_0 + (1 - \Omega_0)\xi]^2 + 1.63 \sigma_{Ry}^{12/10} \Lambda_0 (1 - \xi)^{16/5}. \quad (11)$$

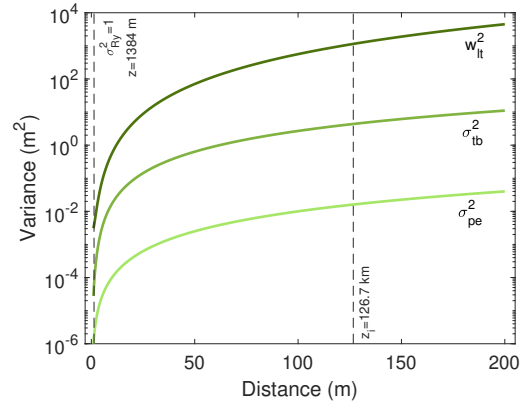


FIG. 1. We compare the variance of the centroid wandering induced by turbulence (σ_{tb}^2 , middle line) to that of pointing error (σ_{pe}^2 , lower line) and the long-term beam waist (w_{lt}^2 , upper line). We assume a collimated beam ($R_0 = +\infty$) with initial radius $w_0 = 5$ cm and wavelength $\lambda = 800$ nm. Other parameters are $L_0 = 1$ m and $C_n^2 = 1.28 \times 10^{-14} \text{ m}^{-2/3}$ (night-time operation). Rytov variance ranges from $\sigma_{Ry}^2 = 1$ at $z = 1384$ m to $\sigma_{Ry}^2 > 9.12 \times 10^3$ at $z = 200$ km.

This is applicable in moderate-to-strong atmospheric turbulence, and is shown to be consistent with experimental data.

As previously discussed, it turns out that centroid wandering is a negligible effect when turbulence is sufficiently strong. In Fig. 1, we plot the turbulence-induced centroid wandering σ_{tb}^2 , the pointing-error wandering σ_{pe}^2 and the long-term beam waist w_{lt}^2 . While at short distances, where $\sigma_{Ry}^2 \sim 1$, they tend towards each other, they diverge at longer distances, where $\sigma_{Ry}^2 \gg 1$. Nevertheless, it is clear that at all distances considered, we have $w_{lt}^2 \gg \sigma_{tb}^2 \gg \sigma_{pe}^2$. In fact, the beam may break up into smaller patches in a very wide area, while the wandering of the centroid becomes negligible.

Turbulence-induced transmissivity. In FSO communication, turbulence can cause power fading and sometimes complete loss of signal. In addition, communication links can experience severe signal degradation as well as spatial/temporal irradiance scintillations in the beam wavefront. To accurately estimate the signal fading and behaviour at some propagation distance, and to learn a true picture of how these affect crucial performance parameters such as the communication rate, it is important to analyze the distribution of the irradiance and/or transmittance at the receiver. In addition, having a theoretical distribution that accurately models these fluctuations under propagation conditions is desirable. This can be achieved through the knowledge of the statistical properties of the intensity fluctuations of the beams. In particular, the probability distribution of the transmittance most thoroughly characterizes the statistics of these fluctuations. Several models have been introduced to deal with this problem, including the log-normal model, the parabolic equation model, Feynman path integral, extended Huygens-Fresnel principle (see Ref. [16]), and the recently proposed elliptic-beam model [37].

The extended Huygens-Fresnel model is considered to be rather easier to use than other methods, especially when it

comes to stronger turbulent media. For a Gaussian beam defined by the set of parameters given in Eqs. (5) and (6), and long-term waist given in Eqs. (7) and (9), the turbulence-induced transmissivity can be computed from

$$\eta_{\text{lt}} = \frac{1}{\mathcal{N}} \int_{\mathcal{A}} d^2r \langle I(r, z) \rangle, \quad (12)$$

where the integration is performed over the area \mathcal{A} of the circular aperture, and

$$\mathcal{N} = \lim_{\mathcal{A} \rightarrow \infty} \int_{\mathcal{A}} d^2r \langle I(r, z) \rangle \quad (13)$$

is a normalization factor. The mean irradiance $\langle I(r, z) \rangle$ is provided by the extended Huygens-Fresnel model [16, Chapt. 7]

$$\langle I(r, z) \rangle = \frac{w_0^2}{w_z^2} \exp \left\{ -\frac{2r^2}{w_z^2} \right\}, \quad z > z_i, \quad (14)$$

and

$$\langle I(r, z) \rangle = \frac{2w_0^2}{w_z^2} \int_0^\infty dt t J_0 \left(\frac{2\sqrt{2}rt}{w_z} \right) e^{-t^2 - yt^{5/3}}, \quad z < z_i, \quad (15)$$

where $J_0(x)$ is a Bessel function and $y = 1.41\sigma_{\text{Ry}}^2\Lambda^{\frac{5}{6}}$.

For $z > z_i$, we replace Eq. (14) in Eqs. (12) and (13). Solving the integration, we can find an explicit analytical form for the transmissivity, given by

$$\eta_{\text{lt}} = 1 - e^{-\frac{2a_R^2}{w_{\text{lt}}^2}}, \quad (16)$$

where w_{lt}^2 is given in Eq. (7). Thus Eq. (16) should be used instead of the pure diffraction transmissivity in Eq. (4).

For $z < z_i$, we cannot find a closed-form but nevertheless we can compute the result numerically by replacing Eq. (15) in Eqs. (12) and (13), and noting that the limit for unlimited area \mathcal{A} can be treated by assuming $a_R = a_R^\infty$ for sufficiently large a_R^∞ . Notwithstanding, we can check that the formula in Eq. (16), where we replace the long-term waist of Eq. (9), provides a limiting lower bound to such numerical values, as shown in Fig. 2. Thus, we may use an analytical expression for the turbulence-induced transmissivity at all distances, as given by Eq. (16) where we replace either Eq. (7) (for $z > z_i$) or Eq. (9) (for $z < z_i$).

Another theoretical model is the log-normal model, where the beam follows a log-normal distribution rather than a Gaussian one. Using this model, we get a similar formula

$$\eta_{\text{lt,LN}} = 1 - e^{-\frac{2a_R^2}{w_{\text{lt,LN}}^2}}, \quad (17)$$

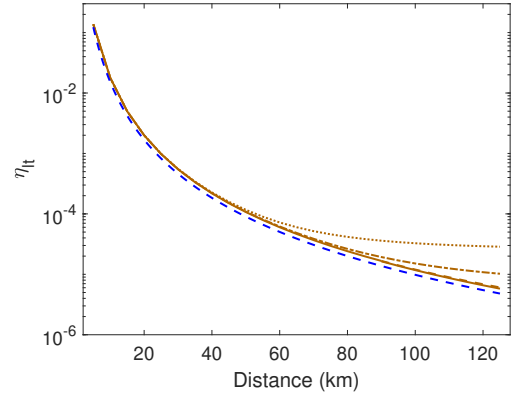


FIG. 2. Turbulence-induced transmissivity versus distance $z < z_i$, where $z_i = 126.7$ km assuming the same parameters of Fig. 1. Brown curves from top to bottom correspond to the Huygens-Fresnel long-term transmissivity numerically computed for $a_R^\infty = 10, 20, 50,$ and 100 m. The lower (dashed blue) curve is the long-term transmissivity analytically computed from Eqs. (16) and (9). The latter can be assumed as limiting lower value at all distances.

where $w_{\text{lt,LN}}^2$ is given in Methods. The validity of the formula holds for all propagation values z and it has been experimentally verified [38]. In addition, it is shown to match recently developed descriptions of atmospheric transmissivity, such as the elliptic-beam model [37]. However, the computation of $w_{\text{lt,LN}}^2$ is cumbersome to handle even numerically. An heuristic choice is to combine Eq. (17) with the calculation of the beam waist from other models, in particular, from the previous Huygens-Fresnel model. Thus, we may consider a *hybrid* log-normal model where we replace $w_{\text{lt,LN}}^2$ with w_{lt}^2 , whose expression is given in Eqs. (7) and (9). This is completely equivalent to the previous approach. For this reason, in our study, we consider η_{lt} of Eq. (16) with long-term waist w_{lt} given by Eqs. (7) and (9).

Bounds and security of quantum communications in a moderate-to-strong turbulent space. Now we are in a position to account for the overall optical loss that can occur in a strong turbulence regime. The overall transmissivity includes the multiplication of three types of optical transmissivity

$$\eta = \eta_{\text{lt}}\eta_{\text{eff}}\eta_{\text{atm}}, \quad (18)$$

where we include the receiver's efficiency η_{eff} and atmospheric loss η_{atm} . The latter is modelled by the Beer-Lambert equation

$$\eta_{\text{atm}} = \exp \left\{ -\alpha(\lambda, h_0)z \right\}, \quad \alpha(\lambda, h_0) = \alpha_0(\lambda)e^{-\frac{h_0}{6600}}, \quad (19)$$

where h_0 is the altitude (measured in metres) and $\alpha_0(\lambda)$ is the extinction factor at sea level [39, 40].

By replacing the combined transmissivity of Eq. (18) in the repeaterless PLOB bound $\Phi(\eta) = -\log_2(1 - \eta)$ [14], one gets the following upper bound for the rate R of any QKD protocol over the FSO link

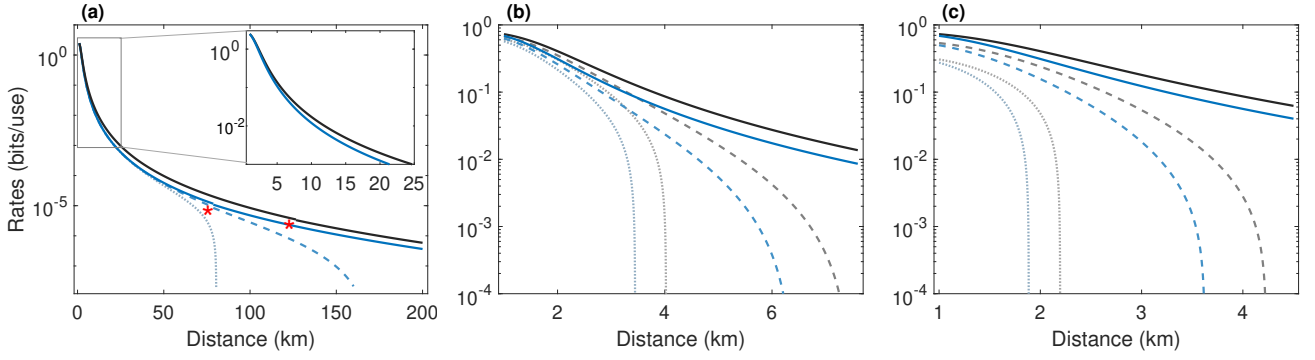


FIG. 3. Free-space optical quantum communications in a moderate-to-strong turbulent space, at night-time (black curves) and day-time (blue curves). In (a) we plot the ultimate pure-loss bound of Eq. (20) with an ideal receiver, $\eta_{\text{eff}} = 1$ and $\bar{n}_{\text{ex}} = 0$, at night-time (solid black curves) and day-time (solid blue curve). The dashed (dotted) curves are thermal upper (achievable lower) bounds for an ideal receiver with $\eta_{\text{eff}} = 1$ but $\bar{n}_{\text{ex}} = 0$ [cf. Eqs. (21) and (22)]. The red star indicates the distance z_i (connecting plots from different equations and therefore presenting small discontinuities). Here, the following set of parameters are considered: $\lambda = 800$ nm, $\alpha_0(\lambda) = 5 \times 10^{-6}$ m $^{-1}$, $w_0 = a_R = 5$ cm, $\Omega_{\text{fov}} = 10^{-10}$ sr, $\Delta t = 10$ ns, $\Delta\lambda = 0.1$ pm, $h_0 = 30$ m, so that $C_n^2 = 1.28$ (2.06) $\times 10^{-14}$ m $^{-2/3}$ for night (day). Also, we have thermal noise $\bar{n}_B = 4.75 \times 10^{-12}$ ($\times 10^{-7}$) photons per mode at night (day). In (b) and (c) we assume a lossy and noisy receiver with $\eta_{\text{eff}} = 0.5$ and, respectively, $\bar{n}_{\text{ex}} = 0.01$ and $\bar{n}_{\text{ex}} = 0.05$. As in panel (a), we compare the pure-loss rates (solid) with the thermal-noise bounds (dashed) and the achievable lower bounds (dotted).

$$R \leq \Phi(\eta) := -\log_2 \left[1 - \eta_{\text{eff}} e^{-\alpha(\lambda, h_0)z} \left(1 - e^{-\frac{2a_R^2}{w_{\text{it}}^2}} \right) \right]. \quad (20)$$

We remark that, as shown in Fig. 1, in the moderate-to-strong turbulence regime ($\sigma_{\text{Ry}}^2 \geq 1$) the variance of long-term beam widening is several orders of magnitude larger than that associated with the centroid wandering. Therefore, we can neglect the short-term fading process and assume a fixed transmissivity between the sender and the detector plane at each distance. This is different from the weak turbulence regime where beam widening and wandering are equally important [23].

Apart from loss, the other key element that must be considered in FSO quantum communications is the number of thermal noise photons, which may find their way into the receiver's aperture. They come from the sky brightness and can also be generated within the receiver itself. To involve the effect of thermal noise into the communications bound, we follow and apply the technique introduced in Ref. [23].

The receiver sees a total mean number of thermal photons equal to $\bar{n} = \eta_{\text{eff}} \bar{n}_B + \bar{n}_{\text{ex}}$, where \bar{n}_B and \bar{n}_{ex} are the number of background thermal photons per mode and extra photons generated within the receiver box, respectively. The number \bar{n}_B depends on several factors coupled to the sky and the receiver. It is given by $\bar{n}_B = \pi \lambda \Gamma_R B_{\lambda}^{\text{sky}} / hc$, where B_{λ}^{sky} is the brightness of the sky, which is in the range of $10^{-6} - 10^{-1}$ Wm $^{-2}$ nm $^{-1}$ sr $^{-1}$ from night to cloudy day [41, 42]. The effects of the receiver is gathered in a single parameter $\Gamma_R = \Delta\lambda \Delta t \Omega_{\text{fov}} a_R^2$, where Ω_{fov} , $\Delta\lambda$, and Δt are the angular field of view, spectral filter, and time window of the detector, respectively. The nominal values that we use in this study are $\Omega_{\text{fov}} = 10^{-10}$ sr, $\Delta\lambda = 0.1$ pm, and $\Delta t = 10$ ns. For a receiver with $a_R = 5$ cm, we estimate $\bar{n}_B = 4.75 \times 10^{-12}$ (10^{-7}) background photons per optical mode at night (day).

The total Alice-Bob FSO link is modelled as a thermal-loss channel with transmissivity η and overall thermal noise \bar{n} . The worst-case scenario is when the eavesdropper (Eve) has control over all the input noise. Such a scenario can be simulated by her using a beam splitter with transmissivity η that combines Alice's signal mode with an input thermal mode with $\bar{n}_e = \bar{n}/(1 - \eta)$ mean photons. We then use the thermal-loss version of the PLOB bound. For $\bar{n} \leq \eta$, the secret key capacity in Eq. (20) can be revised to

$$R \leq K_{\text{UB}}(\eta, \bar{n}) := \Phi(\eta) - \frac{\bar{n}}{1 - \eta} \log_2 \eta - h\left(\frac{\bar{n}}{1 - \eta}\right), \quad (21)$$

where $h(x) = (1 + x) \log_2(1 + x) - x \log_2 x$. One may also find the achievable lower bound given by the reverse coherent information [43, 44], i.e., there is an optimal rate R such that

$$R \geq K_{\text{LB}}(\eta, \bar{n}) := \Phi(\eta) - h\left(\frac{\bar{n}}{1 - \eta}\right). \quad (22)$$

We present numerical simulations of the limits on communication rates in Fig. 3 showing the pure-loss bound of Eq. (20) and the thermal-loss bound of Eqs. (21) and (22). One first, and important, conclusion one may make is that we can obtain positive communication rates even in a strong turbulence regime.

Each curve in Fig. 3(a) is made of two parts because we have used two different equations in our simulation, i.e., Eq. (7) for $z \leq z_i$ and Eq. (9) for $z \geq z_i$. The distance $z = z_i$ is indicated by a red star, which is different for night and day operation (the right is for night). We observe a very slight inconsistency at $z = z_i$, which is due to using different expressions. Notwithstanding it is clear that the second part of the rate after z_i follows exactly the same trend as the first part. In Fig. 3(a) we compare the performances at night

and day with an ideal receiver having $\eta_{\text{eff}} = 1$ and $\bar{n}_{\text{ex}} = 0.431$. For night-time operation all curves coincide because of abso-
lutely low background noise ($\bar{n}_B = 4.75 \times 10^{-12}$). However, for day-time, with $\bar{n}_B = 4.75 \times 10^{-7}$, the deviation between the rates becomes distinct at large link distances, so that the thermal lower bound and upper bound drop at nearly 80 km and 150 km, respectively. Nevertheless the plot suggests that high rates can still be achieved at relatively shorter distances at both night and day.

Then we account for a realistic lossy and noisy receiver with $\eta_{\text{eff}} = 0.5$ and $\bar{n}_{\text{ex}} = 0.01$ in Fig. 3(b), while $\eta_{\text{eff}} = 0.5$ and $\bar{n}_{\text{ex}} = 0.05$ in Fig. 3(c). It is observed that the thermal photons generated at the receiver suppress the rates so that distances are of the order of a few kilometres. As we shall show later, this can be partially alleviated by using a receiver with a larger aperture size.

Long free-space distances that we are considering here, e.g., $z = 100$ km, may not seem so practical, especially because Earth's geometry, in particular its curvature, does not allow two terrestrial stations to actually "see" each other. For example, the maximum distance between two communications towers with height 30 m is about 40 km. Although this can be true for terrestrial stations, we allow for a wider variety of FSO links, including HAPS. Otherwise, a long-distance link could basically be an equivalent section of the atmosphere with a shorter length but stronger turbulence.

Remarkably, the key rates for a moderate-to-strong turbulence regime can be seen as the tail of the rates found in Ref. [23] for weak turbulence. This is where, at about 1384 m distance, we have $\sigma_{\text{Ry}}^2 = 1$ and longer distances induce stronger turbulence regime (for sake of comparison, we have used the same set of parameters used in Ref. [23]). The main reason is that Eq. (9) is sufficiently precise even in weak turbulence regimes. Let us also remark the reason behind choosing $\Delta\lambda = 0.1$ pm, which is discussed in detail in Ref. [23]. Due to the mode-matching properties of coherent receivers such as homodyne detection, where a local oscillator (LO) is involved, we are able to assume a narrow-band filter, as small as $\Delta\lambda = 0.1$ pm (corresponding to the bandwidth $\Delta\nu = 50$ MHz of the LO at $\lambda = 800$ nm). This would suppress the background noise \bar{n}_B to the order of 10^{-12} (10^{-7}) at night (day) time, which in turn allow for positive rates that could not have been obtained otherwise. We refer to Ref. [23] for more detail.

Composable finite-key security analysis. Equation (22) gives the achievable lower bound for key distribution rate when, ideally, an infinite number of signals are used for key extraction. However, in a real-world scenario, communication links can only be used a finite number of times. Hence, we may expect a poorer key rate than the asymptotic one. In addition, the security of a QKD protocol is desirable to be composable, i.e., the protocol must not be distinguished from an ideal protocol which is secure by construction [1]. Mathematically, a composable security proof can be provided by incorporating proper error parameters (ε 's) for each segment of the protocol, namely, error correction, smoothing, and hashing [45, 46]. To address this finiteness and composability, we study a QKD protocol based on coherent states for which we compute the composable finite-size key rate.

We consider the homodyne-based coherent-state QKD protocol [47, 48], the GG02 protocol, where Alice prepares N Gaussian-modulated signals, with variance V , and sends them through a quantum channel to Bob. The latter performs a homodyne measurement, whereby he randomly measures one of the light quadratures. A number n of signals will be used for key extraction, while the rest $m_{\text{pe}} = N - n$ are left for parameter estimation. It can then be shown that the composable finite-size secret key rate is given by [23, 24]

$$R_{\varepsilon} \geq p_{\text{ec}}(1 - r_{\text{pe}}) \left(R_{\text{pe}} - \frac{\Delta_{\text{aep}}}{\sqrt{n}} + \frac{\Omega}{\sqrt{n}} \right), \quad (23)$$

where p_{ec} is the success probability of error correction connected to the frame error rate by $\text{FER} = 1 - p_{\text{ec}}$, $r_{\text{pe}} = m_{\text{pe}}/N$ is the fraction of signals used for parameter estimation, R_{pe} is the asymptotic key rate accounting for parameter estimation, and

$$\Delta_{\text{aep}} := 4 \log_2(2\sqrt{d} + 1) \sqrt{\log_2(18p_{\text{ec}}^{-2}\varepsilon_s^{-4})}, \quad (24)$$

$$\Omega := \log_2[p_{\text{ec}}(1 - \varepsilon_s^2/3)] + 2 \log_2(\sqrt{2}\varepsilon_h). \quad (25)$$

In Eq. (23), the asymptotic rate R_{pe} is calculated for the worst-case values of transmissivity and excess noise to be evaluated at the parameter estimation stage. These values are chosen within w confidence intervals so that they are correct up to an error probability of $\varepsilon_{\text{pe}} = [1 - \text{erf}(w/\sqrt{2})]/2$. See Methods for the calculation of R_{pe} . Equation (23) is valid for a protocol with overall security $\varepsilon = \varepsilon_{\text{cor}} + \varepsilon_s + \varepsilon_h + 2p_{\text{ec}}\varepsilon_{\text{pe}}$ [23], where $\varepsilon_{\text{h(s)}}$ is the hashing (smoothing) parameter and ε_{cor} is the ε_{cor} -correctness bounding the probability that Alice's and Bob's sequences are different even if they pass error correction. Finally, one needs to account for the analog-to-digital conversion so that each continuous-variable symbol is encoded in d bits.

One further consideration regards the measurement techniques in CV-QKD. The received signals can be detected by using a coherent (homodyne or heterodyne) detection with the help of an either transmitted local oscillator (TLO) or local local oscillator (LLO). It turns out that at long distances the amount of detection noise is much lower for the LLO case. But, at the same time, the signal, which propagates through a turbulent path, and the LO, which is produced locally at the receiver, would not be spatially matched. As we show in Methods, this introduces even more loss to the system during the detection process. Therefore, we modify the overall transmissivity in Eq. (18) by a further factor η_{cd} , i.e.,

$$\eta = \eta_{\text{tr}}\eta_{\text{eff}}\eta_{\text{cd}}\eta_{\text{atm}}. \quad (26)$$

Our estimate is that at long distances we roughly have $\eta_{\text{cd}} = 0.63$, which is the value used in our simulation.

Fig. 4 shows the composable finite-size key rate versus (a) block size and (b) receiver aperture size in a strong turbulence space. The link's length is $z = 10$ km, equivalent to 7.84 dB, and the Rytov number is $\sigma_{\text{Ry}}^2 = 37.56$ (60.45) at night (day).

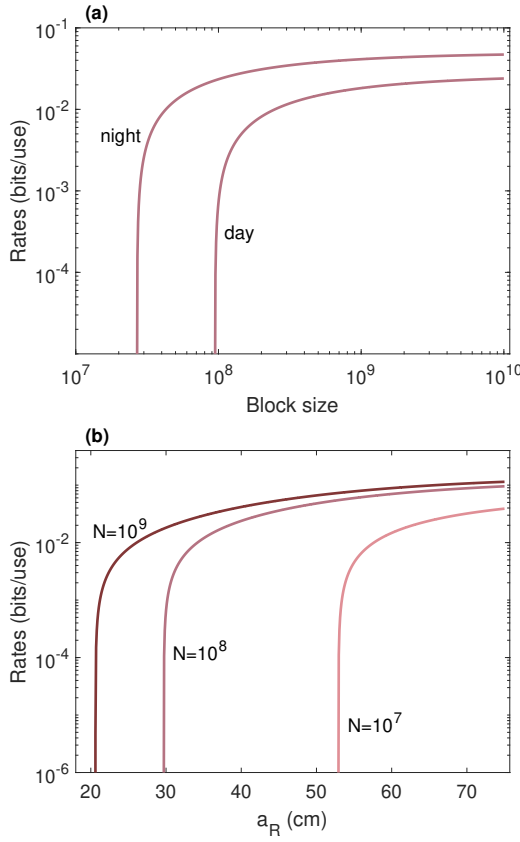


FIG. 4. Numerical results for the composable secret-key rate of a FSO CV-QKD protocol in turbulent space versus (a) block size and (b) receiver aperture size. In (a), an aperture size $a_R = 30$ cm is fixed. In (b), assuming night-time operation, we plot the rate for various block-size values. In both plots we assume a lossy and noisy receiver with $\eta_{\text{eff}} = 0.5$, $\eta_{\text{cd}} = 0.63$, and $\bar{n}_{\text{ex}} = 0.001$. Distance is $z = 10$ km. Other physical parameters are set as given in Fig. 3, except \bar{n}_B which varies with a_R . Protocol parameters are: $\mu = 10$, $r_{\text{pe}} = 0.1$, $d = 2^5$, FER = 0.1, $\varepsilon_s = \varepsilon_h = \varepsilon_{\text{cor}} = 10^{-10}$, $w = 6.34$, $\varepsilon = 4.5 \times 10^{-10}$, and $\beta = 0.98$.

In Fig. 4(a) we have fixed the receiver aperture size to $a_R = 30$ cm. The rates at night-time operation can be obtained with a typical block-size of $\sim 10^8$, while the system demands a larger block-size, which is still acceptable. We observe that one main parameter that substantially affects the rates, at fixed distance and block-size, is the aperture size. From Fig. 4(b) we see that, at fixed length of $z = 10$ km, positive rates can be achieved with a relatively large receiver. However, note that the aperture cannot be made too large. In fact, increasing the receiver size lets more thermal photons into the detection system, e.g., we get $\bar{n}_B = 1.71 \times 10^{-10}$ (10^{-5}) for $a_R = 30$ cm, versus $\bar{n}_B = 4.75 \times 10^{-12}$ (10^{-7}) for $a_R = 5$ cm, at night (day).

Satellite communications at large zenith angles. Here we apply the theory to a satellite communication link beyond 1 rad up to the horizon, where turbulence is strong. In particular, we focus on the mask (or cutoff) angle, θ_m , which is the minimum acceptable elevation above the horizon that a satellite has to be at to avoid blockage of line-of-sight. This is im-

portant because the key rates that will be derived for the mask angle represent lower bounds for the entire satellite quantum communication system. One can set a mask angle that tells the receiver to ignore the satellite at zenith angles larger than θ_m , i.e., lower elevations. The mask angle is roughly 80 deg ($4\pi/9$ rad) that is 10 deg from the horizon.

In this study, we consider a zenith-crossing satellite at altitude h , whose slant distance to the ground station, located at h_0 above sea-level, is given by

$$z = \sqrt{(R_E + h)^2 + (R_E + h_0)^2(\cos^2 \theta - 1)} - (R_E + h_0) \cos \theta, \quad (27)$$

where $R_E \simeq 6370$ km is Earth's radius and θ the zenith angle. To continue, we first need to identify the regime of operation. Replacing the above equation in the Rytov number of Eq. (1) cannot be used for a slant link out to the space because the index-of-refraction structure C_n^2 is not anymore constant and varies with the altitude h . We then require a more general, altitude-dependent, theory that stands as a measure for atmospheric scintillations and the turbulence regime. Assuming a downlink path from space, we take the following expression for scintillation index [49]

$$\sigma_I^2(h > 20 \text{ km}, \theta) = \exp \left[\frac{0.49 \sigma_{\text{Ry}}^2(h, \theta)}{\left(1 + 1.11 \sigma_{\text{Ry}}^{12/5}(h, \theta)\right)^{7/6}} + \frac{0.51 \sigma_{\text{Ry}}^2(h, \theta)}{\left(1 + 0.69 \sigma_{\text{Ry}}^{12/5}(h, \theta)\right)^{5/6}} \right] - 1, \quad (28)$$

where

$$\sigma_{\text{Ry}}^2(h, \theta) = 2.25 k^{\frac{7}{6}} \sec^{\frac{11}{6}}(\theta) \int_{h_0}^h dh' (h' - h_0)^{\frac{5}{6}} C_n^2(h').$$

In fact, $\sigma_I^2(h, \theta)$ is the modified version of a typical Rytov number that is now a function of altitude, zenith angle, as well as varying properties of the atmosphere. According to the Hufnagel-Valley (H-V) atmospheric model [16, Sec. 12.2], the index-of-refraction structure is a function of the altitude

$$C_n^2(h) = 5.94 \times 10^{-53} (\nu/27)^2 h^{10} e^{-h/1000} + 2.7 \times 10^{-16} e^{-h/1500} + A e^{-h/100}, \quad (29)$$

where ν is the windspeed [m/s] and A is the nominal value of $C_n^2(0)$ [$\text{m}^{-2/3}$] at the ground. Note that the above equation gives a good estimate of the index-of-refraction structure only for $h > 20$ km. In our simulation, we consider low-wind night-time by assuming $\nu = 21$ m/s and $A = 1.7 \times 10^{-14} \text{ m}^{-2/3}$, and high-wind day-time by assuming $\nu = 57$ m/s and $A = 2.75 \times 10^{-14} \text{ m}^{-2/3}$ [16, 24].

As it is seen in Fig. 5(a), for zenith angles larger than 1 rad we have $\sigma_I^2 > 1$, which means that signals will experience a moderate/strong turbulent space in such operational regimes.

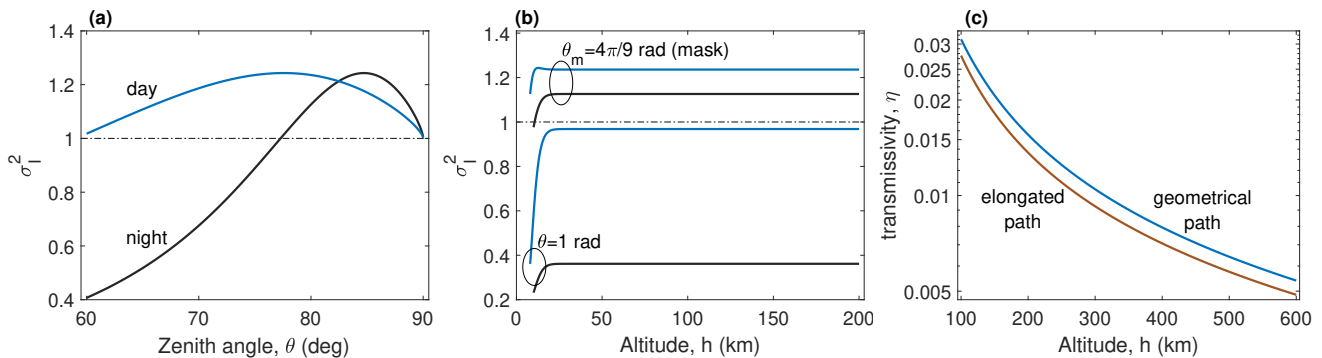


FIG. 5. Satellite communications at large zenith angle. In (a) we show the scintillation index of Eq. (28) versus the zenith angle, at fixed $z = 200$ km. In (b) we plot the scintillation index of Eq. (28) versus altitude h , at $\theta = 1$ rad and $\theta_m = 4\pi/9$ rad. In (a) and (b) black curves are for clear-night turbulence conditions, while blue curves are for day-time and high-wind conditions. In (c) we illustrate the non-trivial difference between the elongated and geometrical paths at the mask angle $\theta_m = 4\pi/9$. In (c) we have set $w_0 = 20$ cm, $a_R = 40$ cm, $\lambda = 800$ nm, $h_0 = 30$, $\alpha_0(\lambda) = 5 \times 10^{-6} \text{ m}^{-1}$, and $\eta_{\text{eff}} = 0.5$.

As $\theta \rightarrow 90$ deg scintillation drops to 1; precisely, to 1.0033. In addition, Fig. 5(b) shows σ_I^2 versus altitude h , at the zenith angle $\theta = 1$ rad as well as at the mask angle $\theta_m = 4\pi/9$ rad. At $\theta = 1$ rad, the turbulence is weak for both night- and day-time operation, as also argued previously in Ref. [24]. Whereas, at relatively high zenith angle, such as a mask angle of 80 deg, the turbulence in the link is strong at all values of altitude $h > 20$ km.

Another important factor that plays a role in a slant satellite path at large zenith angles is geometrical elongation of the communication links. This is due to the refraction on interfaces of atmospheric layers, which introduces even more optical loss. It accounts for the apparent position of celestial objects toward the zenith, and is measured as the elongation factor, which is defined by the quotient of the (bent) optical trajectory and the (direct) geometrical slant path. We account for the elongation factor via the methodology introduced in Ref. [50]. It uses the so-called standard atmosphere model and distinguishes 10 atmospheric layers above the Earth's surface (within each layer the latitude dependence of refractive index is to be assumed linear). In Fig. 5(c), we plot the optical loss for an elongated path, at night and at mask angles $\theta_m = 4\pi/9$ rad, and compare it with that without elongation. It is seen that the elongated path imposes more optical loss.

Let us now apply all the above consideration to the evaluation of finite-size key rates. In Fig. 6(a), for several block-size values, we have plotted key rates at night-time operation and at mask angle $\theta_m = 4\pi/9$ rad, where turbulence is strong (cf. Fig. 5). Here we have set $w_0 = 20$ cm, $a_R = 50$ cm, which constrains $\bar{n}_B = 4.75 \times 10^{-10}$, and $\bar{n}_{\text{ex}} = 0.001$. For the sake of comparison, we have also shown the pure-loss upper bound, which continue to offer higher rates with increasing the satellite altitude, whereas the finite-size rates drop at relatively lower altitudes. Furthermore, in Fig. 6(b), for several altitudes, we have plotted composable finite-size key rates versus block size, at night and at mask angle $\theta_m = 4\pi/9$ rad. Our simulation illustrates that with a reasonable block size quantum satellite communication is feasible for altitudes up to 200km.

SUMMARY

In this work we have extended the field of FSO quantum communications to a moderate-to-strong turbulent space where atmospheric conditions can be harsh and fatal to optical signals. Despite the possibility that the signals could be severely degraded and subjected to high optical loss, our results demonstrated that it is possible to obtain positive key rates. After introducing a figure of merit for the strength of turbulence, we showed that in stronger turbulence regimes the beam spread dominates pointing errors and beam wandering, so that the latter effects can be ignored. We have then justified that the transmissivity estimated by a hybrid log-normal model can safely be used as a lower bound to the more elaborate extended Huygens-Fresnel model.

With these tools in hand, we have computed the ultimate bounds for FSO quantum communication in moderate-to-strong turbulence regimes. Besides establishing these ultimate limits, we have also derived practical and composable finite-key rates for CV-QKD operated in such a strong turbulent space. An important feature is the level of excess noise generated at the receiver which may greatly reduce the key rates and reduce the distance for secure communication. However, our analysis also show that increasing the aperture of the receiver can mitigate the problem and revive the rates. As a main application of our results, we have then investigated satellite quantum communications at large zenith angles, specifically at the mask angle where not only turbulence is strong but also the elongation induced by refraction becomes relevant. This analysis allowed us to show that CV-QKD is feasible even in satellite links affected by strong turbulence, therefore removing the necessity and the restrictions associated with the weak turbulence regime which is at the basis of previous literature.

METHODS

We here present the main techniques that are needed to prove or support the results of our main text.

Transmissivity in a turbulence media: log-normal atmospheric model. In the log-normal model the probability

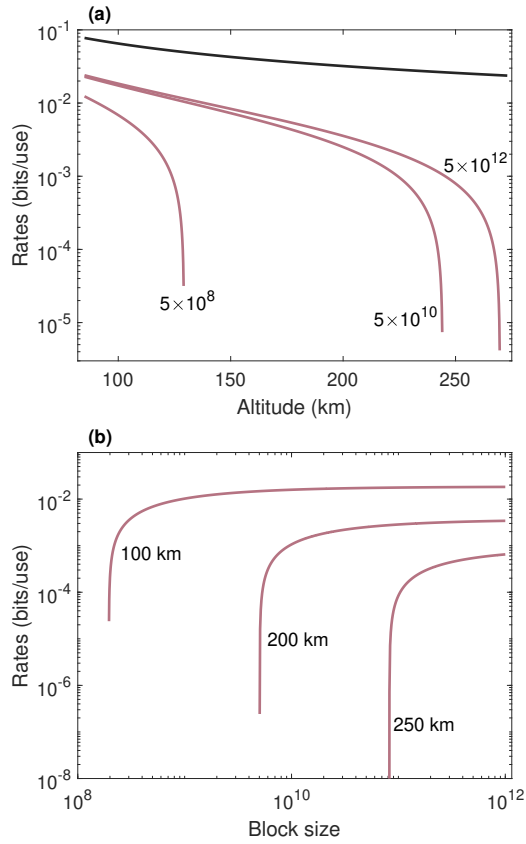


FIG. 6. Performance of satellite quantum communications at large zenith angles. In (a), we have finite-size key rates versus altitude (for fixed values of block-size). In (b) we have similar rates versus block-size (for fixed values of altitude). Both figures consider a mask angle $\theta_m = 4\pi/9$ at night-time, and windspeed $v = 21$ m/s and $A = 1.7 \times 10^{-14} \text{ m}^{-2/3}$ used in Eq. (29). Here we have set $w_0 = 20$ cm, $a_R = 50$ cm, $\bar{n}_B = 4.75 \times 10^{-10}$, $\bar{n}_{\text{ex}} = 0.001$, and $\eta_{\text{cd}} = 0.63$. Other parameters chosen as given in Fig. 5. Protocol parameters are taken as follows: $\mu = 10$, $r_{\text{pe}} = 0.1$, $d = 2^5$, FER = 0.1, $\varepsilon_s = \varepsilon_h = \varepsilon_{\text{cor}} = 10^{-10}$, $w = 6.34$, $\varepsilon = 4.5 \times 10^{-10}$, and $\beta = 0.98$.

distribution for the transmissivity is given by [37]

$$\mathcal{P}(\eta) = \frac{1}{\eta\sigma\sqrt{2\pi}} \exp\left\{-\frac{(-\ln\eta - \mu)^2}{2\sigma^2}\right\}, \quad (30)$$

where $\mu = -\ln(\eta^2/\sqrt{\langle\eta^2\rangle})$ and $\sigma^2 = \ln(\langle\eta^2\rangle/\eta^2)$ are parameters of the log-normal distribution. They are functions of the first and second moments of the transmissivity

$$\eta = \int_{\mathcal{A}} d^2\mathbf{r} \langle I(\mathbf{r}, z) \rangle = \int_{\mathcal{A}} d^2\mathbf{r} \Gamma_2(\mathbf{r}) \quad (31)$$

and

$$\langle \eta^2 \rangle = \int_{\mathcal{A}} d^2\mathbf{r}_1 d^2\mathbf{r}_2 \Gamma_4(\mathbf{r}_1, \mathbf{r}_2), \quad (32)$$

where the integration is performed over the circular aperture opening area \mathcal{A} . In above equations, $\mathbf{r} = (x \ y)^T$ is the vector of transverse coordinates on the receiver plane.

The field coherence functions Γ_2 and Γ_4 are respectively given by [37]

$$\Gamma_2(\mathbf{r}) = \frac{k^2}{4\pi^2 z^2} \int_{\mathbb{R}^2} d^2\mathbf{r}' e^{-\frac{g^2|\mathbf{r}'|^2}{2w_0^2} - 2i\frac{\Upsilon}{w_0^2}\mathbf{r}\cdot\mathbf{r}' - \frac{1}{2}D_S(0, \mathbf{r}')} \quad (33)$$

and

$$\begin{aligned} \Gamma_4(\mathbf{r}_1, \mathbf{r}_2) = & \frac{2k^4}{\pi^2(2\pi)^3 z^4 w_0^2} \int_{\mathbb{R}^6} d^2\mathbf{r}'_1 d^2\mathbf{r}'_2 d^2\mathbf{r}'_3 \\ & \times e^{-\frac{1}{w_0^2}(|\mathbf{r}'_1|^2 + |\mathbf{r}'_2|^2 + |\mathbf{r}'_3|^2)} \\ & \times e^{+2i\frac{\Upsilon}{w_0^2}[(1-z/R_0)\mathbf{r}'_1 \cdot \mathbf{r}'_2 - (\mathbf{r}_1 - \mathbf{r}_2) \cdot \mathbf{r}'_2 - (\mathbf{r}_1 + \mathbf{r}_2) \cdot \mathbf{r}'_3]} \\ & \times \exp\left[\frac{1}{2} \sum_{j=1,2} \left\{ D_S(\mathbf{r}_1 - \mathbf{r}_2, \mathbf{r}'_j + (-1)^j \mathbf{r}'_3) \right. \right. \\ & \left. \left. - D_S(\mathbf{r}_1 - \mathbf{r}_2, \mathbf{r}'_j + (-1)^j \mathbf{r}'_3) - D_S(0, \mathbf{r}'_2 + (-1)^j \mathbf{r}'_3) \right\}\right], \quad (34) \end{aligned}$$

where $\Upsilon = kw_0^2/(2z)$ is the Fresnel number of the transmitter aperture and $g^2 = 1 + \Upsilon^2(1 - z/R_0)^2$ is the generalized diffraction beam parameter. Here,

$$D_S(\mathbf{r}, \mathbf{r}') = 2\rho_0^{-5/3} \int_0^1 d\xi |\mathbf{r}\xi + \mathbf{r}'(1-\xi)|^{5/3} \quad (35)$$

is the phase structure function, where ρ_0 is the radius of spatial coherence of the wave in the atmosphere.

The first moment of the transmissivity in Eq. (31) can be evaluated explicitly

$$\eta = 1 - e^{-\frac{2a_R^2}{w_{\text{it,LN}}^2}}, \quad (36)$$

where

$$\begin{aligned} w_{\text{it,LN}}^2 = & S_{xx} + 4\langle x_0^2 \rangle \\ \equiv & w_{\text{st,LN}}^2 + \sigma_{\text{tb}}^2 \end{aligned} \quad (37)$$

is the long-term beam size, with

$$\begin{aligned} S_{xx} = & 4 \left[\int_{\mathbb{R}^2} d^2\mathbf{r} x^2 \Gamma_2(\mathbf{r}, z) \right. \\ & \left. - \int_{\mathbb{R}^4} d^2\mathbf{r}_1 d^2\mathbf{r}_2 x_1 x_2 \Gamma_4(\mathbf{r}_1, \mathbf{r}_2, z) \right] \quad (38) \end{aligned}$$

627 and

$$\langle x_0^2 \rangle = \int_{\mathbb{R}^4} d^2 r_1 d^2 r_2 x_1 x_2 \Gamma_4(r_1, r_2, z). \quad (39)$$

628 **Extra photons generated within the receiver.** Considering
629 a CV-QKD experiment, there are two techniques whereby
630 one can measure the received signals through a coherent (homo-
631 dyne or heterodyne) detection: transmitted local oscillator
632 (TLO) and local local oscillator (LLO). In Ref. [23, 24], it is
633 shown that these two may lead to generating totally different
634 amounts of noisy photons within the coherent receiver system.
635 This is mostly because extra photons generated by LLO, $\bar{n}_{\text{ex}}^{\text{LLO}}$,
636 is a linear function of the link transmissivity, η , whereas extra
637 photons generated by TLO, $\bar{n}_{\text{ex}}^{\text{TLO}}$, is an inverse function of it.
638 Precisely, it reads [23, Eq. (62)]

$$\bar{n}_{\text{ex}}^{\text{LLO}} = \Theta + \pi\eta V_A l_w C^{-1} \text{ and } \bar{n}_{\text{ex}}^{\text{TLO}} = \frac{\Theta}{\eta}, \quad (40)$$

639 where

$$\Theta = \frac{\nu_{\text{det}} \text{NEP}^2 \lambda W \Delta t_{\text{LO}}}{2hc P_{\text{LO}}}, \quad (41)$$

640 with h being the Planck constant and c the speed of light.
641 Also, V_A is the modulation variance, P_{LO} the LO power, C
642 the clock, l_w the linewidth, W the detector bandwidth, NEP
643 the noise equivalent power, Δt_{LO} the LO pulse duration, and
644 ν_{det} the detection noise variance— $\nu_{\text{det}} = 1(2)$ for a homodyne
645 (heterodyne) measurement. We refer to Ref. [23] for more
646 detail.

647 In Fig. 7, we plot \bar{n}_{ex} versus distance. As seen at rela-
648 tively large distances, i.e., the regime of strong turbulence,
649 the LLO technique is the better detection scheme. However,
650 the quality of LLO detection may be poorer due to overlap-
651 ping a fresh LO with the signal. In TLO, both the signal and
652 the LO undergo the same (atmospheric turbulent) conditions,
653 so that when they are recombined at the receiver, ideally, no
654 mismatch is expected. This is not the case of LLO which we
655 discuss in more detail in the following.

656 **LLO-induced loss.** Suppose two continuous wave optical
657 beams—the signal E_S and the LO E_L —of the same frequency
658 are incident on a beam splitter τ . Let us consider a balanced
659 homodyne detection, i.e., $\tau = 1/\sqrt{2}$, where the output number
660 of photons is given by [21, 51]

$$n_- = \eta_{\text{eff}} \int_0^T dt \int_{\mathcal{A}} d^2 r [E_L^-(r, z, t) E_S^+(r, z, t) + E_S^-(r, z, t) E_L^+(r, z, t)], \quad (42)$$

661 with spatial-temporal modes defined as follows

$$E_S^+(r, z, t) = i\hat{a}_S f_S(t) u_S(r, z), E_L^+(r, z, t) = i\hat{a}_L f_L(t) u_L(r, z), \quad (43)$$

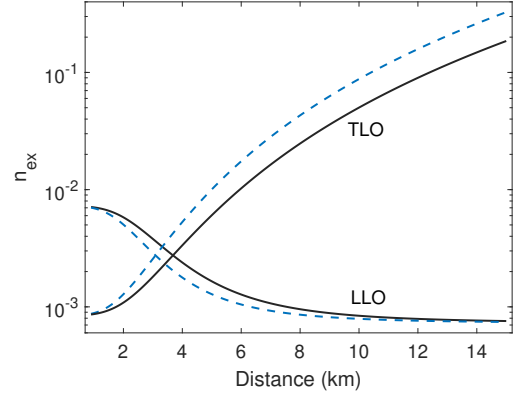


FIG. 7. Extra noise photons generated within a coherent receiver (homodyne detection), at night (solid black curves) and day (dashed blue curves) where a TLO/LLO technique is used. We have $\nu_{\text{det}} = 1$ SNU, $\text{NEP} = 6 \text{ pW}/\sqrt{\text{Hz}}$, $W = 100 \text{ MHz}$, $\Delta t_{\text{LO}} = 10 \text{ ns}$, $P_{\text{LO}} = 100 \text{ mW}$, $V_A = 8 \text{ SNU}$, $l_w = 1.6 \text{ KHz}$, $C = 5 \text{ MHz}$, and $hc = 1.986 \times 10^{-25} \text{ J.m}$. Other parameters related to η are set as in Fig. 3.

662 and \hat{a} being the corresponding annihilation operator.

663 Usually, for quantum tomography purposes and phase-
664 sensitive detection, the LO field is assumed a monochro-
665 matic coherent state, with the on-axis amplitude $|\alpha_L|$, $f_L(t) = e^{-i\omega t}$, and $u_L(r, 0)e^{i\phi_L}$ (plane wave) or $u_L(r, 0) = e^{ikr}$ (spherical wave) [21, 51–53]. This then follows

$$n_- \propto \eta_{\text{eff}} |\alpha_L| (\hat{a}_S e^{i\Delta\phi} + \hat{a}_S^\dagger e^{-i\Delta\phi}) = \eta_{\text{eff}} |\alpha_L| \hat{q}_S(\Delta\phi), \quad (44)$$

666 where $\hat{q}_S(\Delta\phi)$ is signal's quadrature with $\Delta\phi = \phi_S - \phi_L$.

667 Back to the the coherent detection in a free-space scenario,
668 in the following we show that some loss is expected in the case
669 of LLO, where signal's shape is different from that of the LO.
670 We consider coherent Gaussian beams, which in the plane of
671 the exit aperture of the transmitter are described by

$$u(r, 0) = e^{-\frac{r^2}{w_0^2} - \frac{ikr^2}{2R_0}}, \quad (45)$$

672 where w_0 is the beam spot radius and R_0 is its phase front
673 radius of curvature. For simplicity, we assume a collimated
674 beam with $R_0 \rightarrow \infty$, such that

$$u(r, 0) = e^{-\frac{r^2}{w_0^2}}. \quad (46)$$

675 At distance z a Gaussian beam may or may not keep its Gaus-
676 sian form. If it does, the beam width w_0 will be replaced
677 with $W(z)$ —short- or long-term beam size according to the
678 turbulence regime. However, in general, $u(r, z)$ can be dis-
679 torted, or even completely destroyed, during a turbulent path.
680 In that case, proper functions $u(r, z)$ should be used that re-
681 flect the effects of turbulence. We assume far-field conditions
682 where Gaussian beams can be approximated by plane waves
683 [16]. Therefore, in the case of TLO, the signal and the LO
684

can be taken as plane waves that reduces the problem to previous (usual) coherent detection scenarios [21, 51–53], with the expectation value of photocurrent from Eq. (42) as follows

$$\langle n_- \rangle_{\text{TLO}} \propto \eta_{\text{eff}} |\alpha_S(z)| |\alpha_L(z)| \cos(\Delta\phi). \quad (47)$$

When it comes to LLO, we should consider the Gaussian shape of the fresh LO generated locally at the receiver, while we assume the signal has the form of a plane wave. By replacing Eq. (46) for the LO into Eq. (42), and assuming that signal and the LO are frequency matched, it is straightforward to find

$$\langle n_- \rangle_{\text{LLO}} \propto \eta_{\text{eff}} |\alpha_S(z)| |\alpha_L(0)| \cos(\Delta\phi) \frac{1}{\mathcal{N}_0} \int_{\mathcal{A}} dr re^{-\frac{r^2}{w_L^2(0)}}, \quad (48)$$

which is also normalized by $\mathcal{N}_0 = \int_{\mathcal{A} \rightarrow \infty} dr re^{-\frac{r^2}{w_L^2(0)}}$ (the receiver does not collect all the light). It is evident that the expression

$$\eta_{\text{LLO}} := \frac{1}{\mathcal{N}_0} \int_{\mathcal{A}} dr re^{-\frac{r^2}{w_L^2(0)}} \quad (49)$$

has the same nature as the quantum efficiency of the detectors η_{eff} ; hence, can be considered as extra loss. One can implicitly find that

$$\eta_{\text{LLO}} = 1 - e^{-\frac{a_R^2}{w_L^2(0)}}. \quad (50)$$

For the special case where the aperture size (or equivalently the lenses that collect and focus the beam on the detection's beam splitter) is equal to the LO's initial size, we have $\eta_{\text{LLO}} = 1 - e^{-1} = 0.63$.

The overall transmissivity can then be written as follows

$$\eta = \eta_{\text{lt}} \eta_{\text{eff}} \eta_{\text{cd}} \eta_{\text{atm}}, \quad (51)$$

where η_{cd} represents η_{TLO} or η_{LLO} . In our estimation of composable CV-QKD rates, we use $\eta_{\text{cd}} = 0.63$.

We remark that a more precise evaluation involves working out a more precise shape of the beam after propagating through a turbulent medium, where $u_{S/LO}(r, z)$ functions that include the effects of turbulent are known. One possible procedure is as follows: due to the extended Huygens-Fresnel principle the optical wave field after propagating a distance z through a turbulent space is given by solving [16, Eq. (21) Chapt. 7], where the most complex function seems to be the *complex phase perturbation* of the field [54, 55]. One can then compute a more accurate loss coherent detection η_{cd} from the above methodology.

Details of key rate analysis and parameter estimation. For the secret key rate analysis we use consider the

entanglement-based representation of the coherent-state QKD protocol. We assume a collective Gaussian entangling-cloner attack [56]. At each run of the protocol Alice shares one leg of a two-mode squeezed vacuum (TMSV) state, with variance μ , through a communications link with Bob. This is equivalent to the prepare and measure version of the protocol, where Alice prepares coherent states by a bivariate Gaussian modulation with variance $\sigma_x^2 = \mu - 1$. Assuming that the link is a thermal-loss channel, characterized by the transmissivity η and thermal noise \bar{n} , the end-to-end covariance matrix between Alice and Bob has the form

$$\mathbf{V}_{AB} = \begin{pmatrix} a\mathbb{1} & c\mathbb{Z} \\ c\mathbb{Z} & b\mathbb{1} \end{pmatrix}, \quad (52)$$

where $a = \mu$, $b = \eta(\mu - 1) + 2\bar{n} + 1$, $c = \sqrt{\eta(\mu^2 - 1)}$, $\mathbb{1} = \text{diag}(1, 1)$ and $\mathbb{Z} = \text{diag}(1, -1)$.

Having the triplet (a, b, c) , and assuming a homodyne measurement at Bob's side, the asymptotic key rate in the reverse reconciliation case is given by

$$R_{\text{asy}}(\eta, \bar{n}) = \beta I_{AB}(\eta, \bar{n}) - \chi_{EB}(\eta, \bar{n}) \quad (53)$$

where

$$I_{AB}(\eta, \bar{n}) = \frac{1}{2} \log_2 \left(1 + \frac{\eta(\mu - 1)}{2\bar{n} + 1} \right), \quad (54)$$

Also, assuming that the eavesdropper purifies the entangled state between Alice and Bob, one finds

$$\chi_{BE}(\eta, \bar{n}) = h\left(\frac{\nu_+ - 1}{2}\right) + h\left(\frac{\nu_- - 1}{2}\right) - h\left(\frac{\nu_c - 1}{2}\right). \quad (55)$$

with $h(x)$ given in the main text, $\nu_{\pm} = (\sqrt{(a+b)^2 - 4c^2} \pm (b-a))/2$, and $\nu_c = \sqrt{a(ab - c^2)}/b$.

In a realistic setting, Alice and Bob should compute the values of η and \bar{n} in order to estimate the key rate in Eq. (53). This computation is carried out by using only a finite number of runs, which inevitably reduces the rate to $R_{\text{pe}}(\eta_{\text{wc}}, \bar{n}_{\text{wc}})$, for the worst-case values are $\eta_{\text{wc}} \leq \eta$ and $\bar{n}_{\text{wc}} \geq \bar{n}$ [57, 58].

Before discussing the worst-case scenario parameters, let us point out a matter that eases the parameter estimation in the case of moderate-to-strong turbulence. Unlike the case of a weak turbulence medium [23], where the link transmissivity varies instantaneously, we can assume a fixed loss and a fixed number of thermal photons in the moderate-to-strong turbulence regime due to the fact that beam wandering is negligible here; see Fig. 1. Therefore, we assume a thermal-loss channel that is characterised by transmissivity η and mean number of thermal photons \bar{n} . This channel induces an input-output relation $y = \sqrt{\eta}x + z$ between the input Gaussian variable x and the output variable y , with z being a Gaussian noise variable; the variables x and z have zero mean with variances $\mu - 1$ and $\sigma_z^2 = 2\bar{n} + 1$, respectively.

761 Back to the estimation of the worst-case parameters, by re-774
 762 vealing m pairs of corresponding data, i.e., $[x]_i$ and $[y]_i$, Al-
 763 ice and Bob can build an estimator \hat{T} of the square root of
 764 transmissivity $T = \sqrt{\eta}$, that is $\hat{T} := m^{-1} \sigma_x^{-2} \sum_{i=1}^m x_i y_i$, with
 765 variance $\text{Var}(\hat{T}) = m^{-1} (2\eta + \sigma_x^{-2} \sigma_z^2)$, where $\sigma_x^2 = \sum_{i=1}^m x_i^2 \simeq$
 766 $\mu - 1$. Then, the estimator for transmissivity is $\hat{\eta} = (\hat{T})^2$, with
 767 variance $\text{Var}(\hat{\eta}) = 4m^{-1} \eta^2 (2 + \eta^{-1} \sigma_x^{-2} \sigma_z^2) + \mathcal{O}(m^{-2})$. Sim-776
 768 ilarly, Alice and Bob can construct the estimator for \bar{n} , that
 769 is, $\hat{\bar{n}} := (\hat{\sigma}_z^2 - 1)/2$, with variance $\text{Var}(\hat{\bar{n}}) = \sigma_z^4/(2m)$. Here,
 770 $\hat{\sigma}_z^2 = m^{-1} \sum_{i=1}^m z_i^2$ is the estimator for the variance of the
 771 thermal noise σ_z^2 .

772 Next, by assuming a certain number w of confidence of in-783
 773 tervals, Alice and Bob compute the worst-case estimators up784

to some probability of error $\varepsilon_{\text{pe}} = [1 - \text{erf}(w/\sqrt{2})]/2$, i.e.,

$$\eta_{\text{wc}} = \eta - 2w \sqrt{\frac{2\eta^2 + \eta \sigma_x^{-2} \sigma_z^2}{m}}, \quad \bar{n}_{\text{wc}} = \bar{n} + w \frac{\sigma_z^2}{\sqrt{2m}}. \quad (56)$$

Data availability. All data in this paper can be reproduced by using the methodology described.

Code availability. Code is available upon reasonable request to the authors.

Acknowledgements. This work has been funded by the European Union via ‘‘Continuous Variable Quantum Communications’’ (CiViQ, Grant Agreement No. 820466).

- 785 [1] S. Pirandola, U. L. Andersen, L. Banchi, M. Berta, D. Bunan-827
 786 dar, R. Colbeck, D. Englund, T. Gehring, C. Lupo, C. Ottaviani,828
 787 J. L. Pereira, M. Razavi, J. S. Shaari, M. Tomamichel, V. C.829
 788 Usenko, G. Vallone, P. Villoresi, and P. Wallden, *Adv. Opt.*830
 789 *Photon.* **12**, 1012 (2020). 831
- 790 [2] C. H. Bennett and G. Brassard, in *Proceedings of IEEE Interna-832*
 791 *tional Conference on Computers, Systems, and Signal Process-*833
 792 *ing* (IEEE, New York, Bangalore, India, 1984) pp. 175–179. 834
- 793 [3] J.-P. Chen, C. Zhang, Y. Liu, C. Jiang, W. Zhang, X.-L. Hu,835
 794 J.-Y. Guan, Z.-W. Yu, H. Xu, J. Lin, M.-J. Li, H. Chen, H. Li,836
 795 L. You, Z. Wang, X.-B. Wang, Q. Zhang, and J.-W. Pan, *Phys.*837
 796 *Rev. Lett.* **124**, 070501 (2020). 838
- 797 [4] Q. Zhang, F. Xu, Y.-A. Chen, C.-Z. Peng, and J.-W. Pan, *Opt.*839
 798 *Express* **26**, 24260 (2018). 840
- 799 [5] M. Lucamarini, Z. L. Yuan, J. F. Dynes, and A. J. Shields,841
 800 *Nature* **557**, 400 (2018). 842
- 801 [6] M. Pittaluga, M. Minder, M. Lucamarini, M. Sanzaro, R. I.843
 802 Woodward, M.-J. Li, Z. Yuan, and A. J. Shields, ‘‘600 km844
 803 repeater-like quantum communications with dual-band stabil-845
 804 isation,’’ (2020), arXiv:2012.15099. 846
- 805 [7] H. J. Kimble, *Nature* **453**, 1023 (2008). 847
- 806 [8] S. Pirandola and S. L. Braunstein, *Nature* **532**, 169 (2016). 848
- 807 [9] R. Ursin, F. Tiefenbacher, T. Schmitt-Manderbach, H. Weier,849
 808 T. Scheidl, M. Lindenthal, B. Blauensteiner, T. Jennewein,850
 809 J. Perdigues, P. Trojek, B. Ömer, M. Fürst, M. Meyen-851
 810 burg, J. Rarity, Z. Sodnik, C. Barbieri, H. Weinfurter, and852
 811 A. Zeilinger, *Nature Phys* **3**, 481 (2007). 853
- 812 [10] S.-K. Liao, W.-Q. Cai, W.-Y. Liu, L. Zhang, Y. Li, J.-G. Ren,854
 813 J. Yin, Q. Shen, Y. Cao, Z.-P. Li, F.-Z. Li, X.-W. Chen, L.-855
 814 H. Sun, J.-J. Jia, J.-C. Wu, X.-J. Jiang, J.-F. Wang, Y.-M.856
 815 Huang, Q. Wang, Y.-L. Zhou, L. Deng, T. Xi, L. Ma, T. Hu,857
 816 Q. Zhang, Y.-A. Chen, N.-L. Liu, X.-B. Wang, Z.-C. Zhu, C.-Y.858
 817 Lu, R. Shu, C.-Z. Peng, J.-Y. Wang, and J.-W. Pan, *Nature* **549**,859
 818 43 (2017). 860
- 819 [11] J.-G. Ren, P. Xu, H.-L. Yong, L. Zhang, S.-K. Liao, J. Yin,861
 820 W.-Y. Liu, W.-Q. Cai, M. Yang, L. Li, K.-X. Yang, X. Han,862
 821 Y.-Q. Yao, J. Li, H.-Y. Wu, S. Wan, L. Liu, D.-Q. Liu, Y.-W.863
 822 Kuang, Z.-P. He, P. Shang, C. Guo, R.-H. Zheng, K. Tian, Z.-C.864
 823 Zhu, N.-L. Liu, C.-Y. Lu, R. Shu, Y.-A. Chen, C.-Z. Peng, J.-Y.865
 824 Wang, and J.-W. Pan, *Nature* **549**, 70 (2017). 866
- 825 [12] S.-K. Liao, H.-L. Yong, C. Liu, G.-L. Shentu, D.-D. Li, J. Lin,867
 826 H. Dai, S.-Q. Zhao, B. Li, J.-Y. Guan, W. Chen, Y.-H. Gong,868
- Y. Li, Z.-H. Lin, G.-S. Pan, J. S. Pelc, M. M. Fejer, W.-Z. Zhang, W.-Y. Liu, J. Yin, J.-G. Ren, X.-B. Wang, Q. Zhang, C.-Z. Peng, and J.-W. Pan, *Nature Photon* **311**, 509 (2017).
- [13] J. S. Sidhu, S. K. Joshi, M. Gundogan, T. Brougham, D. Lown-
 des, L. Mazzarella, M. Krutzik, S. Mohapatra, D. Dequal,
 G. Vallone, P. Villoresi, A. Ling, T. Jennewein, M. Mohageg,
 J. Rarity, I. Fuentes, S. Pirandola, and D. K. L. Oi, ‘‘Advances in
 space quantum communications,’’ (2021), arXiv:2103.12749.
- [14] S. Pirandola, R. Laurenza, C. Ottaviani, and L. Banchi, *Nature
 Commun* **8**, 15043 (2017).
- [15] S. Pirandola, *Commun Phys* **2**, 51 (2019), see also preprint
 arXiv:1601.00966 (2016).
- [16] L. C. Andrews and R. L. Phillips, *Laser Beam Propagation
 Through Random Medium*, 2nd ed. (SPIE, 2005).
- [17] H. Kaushal, V. K. Jain, and S. Kar, *Free Space Optical Com-
 munication* (Springer, New York, 2017).
- [18] J. W. Goodman, *Statistical Optics* (John Wiley & Sons, Inc.,
 1985).
- [19] A. Siegman, *Lasers* (University Science Books, 1986).
- [20] O. Svelto, *Principles of Lasers*, 5th ed. (Springer, New York,
 2010).
- [21] D. L. Fried, *Proceedings of the IEEE* **55**, 57 (1967).
- [22] S. S. R. Murty, *Proc. Indian Acad. Sci. (Engg. Sci.)* **2**, 179
 (1979).
- [23] S. Pirandola, *Phys. Rev. Research* **3**, 013279 (2021).
- [24] S. Pirandola, *Phys. Rev. Research* **3**, 023130 (2021).
- [25] R. L. Fante, *Proceedings of the IEEE* **63**, 1669 (1975).
- [26] V. L. Mironov and V. V. Nosov, *J. Opt. Soc. Am.* **67**, 1073
 (1977).
- [27] H. T. Yura, *J. Opt. Soc. Am.* **63**, 567 (1973).
- [28] V. I. Klyatskin and A. I. Kon, *Radiophysics Quantum Electron*
15, 1056 (1972).
- [29] J. R. Kerr and J. R. Dunphy, *J. Opt. Soc. Am.* **63**, 1 (1973).
- [30] H. Raidt and D. H. Höhn, *Appl. Opt.* **14**, 2747 (1975).
- [31] L. C. Andrews, R. L. Phillips, and C. Y. Hopen, *Laser Beam
 Scintillation with Applications*, 2nd ed. (SPIE, 2001).
- [32] S. M. Rytov, *Izvestiya Akademii Nauk SSSR, Seriya Fizich-
 eskaya* (Bulletin of the Academy of Sciences of the USSR,
 Physical Series) **2**, 223 (1937).
- [33] A. Sommerfeld, *International Congress of Mathematicians* **3**,
 116 (1908).
- [34] M. J. Rhodes, *Introduction to Particle Technology*, 2nd ed.

- (John Wiley & Sons Ltd., 2008).
 [35] H. T. Yura, *Appl. Opt.* **10**, 2771 (1971).
 [36] L. C. Andrews, W. B. Miller, and J. C. Ricklin, *J. Opt. Soc. Am. A* **11**, 1653 (1994).
 [37] D. Vasylyev, A. A. Semenov, and W. Vogel, *Phys. Rev. Lett.* **117**, 090501 (2016).
 [38] I. Capraro, A. Tomaello, A. Dall'Arche, F. Gerlin, R. Ursin, G. Vallone, and P. Villoresi, *Phys. Rev. Lett.* **109**, 200502 (2012).
 [39] S. Q. Duntley, *J. Opt. Soc. Am.* **38**, 179 (1948).
 [40] C. F. Bohren and D. R. Huffman, *Absorption and scattering of light by small particles* (John Wiley & Sons Inc., 2008).
 [41] M. Er-long, H. Zheng-fu, G. Shun-sheng, Z. Tao, D. Da-sheng, and G. Guang-can, *New Journal of Physics* **7**, 215 (2005).
 [42] C. Liorni, H. Kampermann, and D. Bruß, *New Journal of Physics* **21**, 093055 (2019).
 [43] R. García-Patrón, S. Pirandola, S. Lloyd, and J. H. Shapiro, *Phys. Rev. Lett.* **102**, 210501 (2009).
 [44] S. Pirandola, R. García-Patrón, S. L. Braunstein, and S. Lloyd, *Phys. Rev. Lett.* **102**, 050503 (2009).
 [45] M. Tomamichel, C. C. W. Lim, N. Gisin, and R. Renner, *Nature Commun* **3**, 634 (2012).
 [46] F. Furrer, T. Franz, M. Berta, A. Leverrier, V. B. Scholz, M. Tomamichel, and R. F. Werner, *Phys. Rev. Lett.* **109**, 100502 (2012).
 [47] F. Grosshans and P. Grangier, *Phys. Rev. Lett.* **88**, 057902 (2002).
 [48] F. Grosshans, G. Van Assche, J. Wenger, R. Brouri, N. J. Cerf, and P. Grangier, *Nature* **421**, 238 (2003).
 [49] L. C. Andrews, R. L. Phillips, and C. Y. Young, *Optical Engineering* **39**, 3272 (2000).
 [50] D. Vasylyev, W. Vogel, and F. Moll, *Phys. Rev. A* **99**, 053830 (2019).
 [51] M. G. Raymer, J. Cooper, H. J. Carmichael, M. Beck, and D. T. Smithey, *J. Opt. Soc. Am. B* **12**, 1801 (1995).
 [52] U. Leonhardt, *Measuring the Quantum State of Light* (Cambridge University Press, Cambridge, 1997).
 [53] D. W. G. J. Milburn, *Quantum Optics*, 2nd ed. (Springer, Berlin, 2008).
 [54] R. F. Lutomirski and H. T. Yura, *Appl. Opt.* **10**, 1652 (1971).
 [55] H. T. Yura and S. G. Hanson, *J. Opt. Soc. Am. A* **6**, 564 (1989).
 [56] S. Pirandola, S. L. Braunstein, and S. Lloyd, *Phys. Rev. Lett.* **101**, 200504 (2008).
 [57] L. Ruppert, V. C. Usenko, and R. Filip, *Phys. Rev. A* **90**, 062310 (2014).
 [58] L. Ruppert, C. Peuntinger, B. Heim, K. Günthner, V. C. Usenko, D. Elser, G. Leuchs, R. Filip, and C. Marquardt, *New Journal of Physics* **21**, 123036 (2019).